frontiers | Frontiers in Energy Research

ORIGINAL RESEARCH
published: 26 April 2022
doi: 10.3389/fenrg.2022.867734

Heat Transfer Evaluation in $MgZn_6Zr/C_8H_{18}$ [(Magnesium–Zinc–Zirconium)/Engine Oil] With Non-linear Solar Thermal Radiations and Modified Slip Boundaries Over a 3-Dimensional Convectively Heated Surface

Adnan[1]*, *Umar Khan*[2], *Naveed Ahmed*[3], *Ilyas Khan*[4], *Abdullah Mohamed*[5] and *Sadok Mehrez*[6,7]

[1]Department of Mathematics, Mohi-ud-Din Islamic University, Nerian Sharif, Pakistan, [2]Department of Mathematics and Statistics, Hazara University, Mansehra, Pakistan, [3]Department of Mathematics, Faculty of Sciences, HITEC University, Taxila Cantt, Pakistan, [4]Department of Mathematics, College of Science Al-Zulfi, Majmaah University, Al-Majmaah, Saudi Arabia, [5]Research Centre, Future University in Egypt, New Cairo, Egypt, [6]Department of Mechanical Engineering, College of Engineering at Al Kharj, Prince Sattam bin Abdulaziz University, Al-Kharj, Saudi Arabia, [7]Department of Mechanical Engineering, University of Tunis El Manar, Tunis, Tunisia

OPEN ACCESS

Edited by:
Hsien-Yi (Sam) Hsu,
City University of Hong Kong, Hong Kong SAR, China

Reviewed by:
M. M. Bhatti,
Shandong University of Science and Technology, China
Iskander Tlili,
Monastir, Tunisia

***Correspondence:**
Adnan
adnan_abbasi89@yahoo.com

Specialty section:
This article was submitted to Solar Energy, a section of the journal Frontiers in Energy Research

Received: 01 February 2022
Accepted: 10 March 2022
Published: 26 April 2022

Citation:
Adnan, Khan U, Ahmed N, Khan I, Mohamed A and Mehrez S (2022) Heat Transfer Evaluation in $MgZn_6Zr/C_8H_{18}$ [(Magnesium–Zinc–Zirconium)/Engine Oil] With Non-linear Solar Thermal Radiations and Modified Slip Boundaries Over a 3-Dimensional Convectively Heated Surface. Front. Energy Res. 10:867734. doi: 10.3389/fenrg.2022.867734

This analysis is concerned about the thermal performance of $[(MgZn_6Zr)/C_8H_{18}]_{nf}$ by incorporating the essential concept of non-linear thermal radiations. The flow is configured over a 3D stretchable surface which is heated convectively and the surface boundaries updated with slip effects; uniform suction is applied. The proper mathematical modeling is performed by exercising the nanofluids' empirical correlations and similarity equations. Thereafter, the RK scheme is utilized to execute the problem solution. The influences of imperative flow constraints are furnished and discussed deeply. The results revealed that $[(MgZn_6Zr)/C_8H_{18}]_{nf}$ motion decays against suction (R_1) and slip effects (γ_1). The investigation of the results disclosed that the induction of non-linear thermal radiations in the model boosted the internal energy of the fluid, and hence, the nanofluid thermal efficiency improved. Moreover, convection provided from the surface (B_i number) was also of paramount interest regarding the heat transport in $[(MgZn_6Zr)/C_8H_{18}]_{nf}$. Furthermore, significant contribution of the temperature ratio parameter β_w is examined in thermal enhancement. Optimum shear stress trends are investigated due to suction from the surface. Finally, we hoped that the problem would be beneficial in the field of applied thermal engineering, more specifically in the heat transport models.

Keywords: heat transfer, $(MgZn_6Zr)/C_8H_{18}$ nanofluid, thermal radiation, velocity slip, convective heat

INTRODUCTION

Nanotechnology is the most progressive and potential research area in the modern technological world. The nanoparticles of various metallic/non-metallic ferrites, CNTs, oxides, and alloys are the key ingredients in nanotechnology. In this loop, nanofluids are also imperatively contributed in the nanotechnological world. These are fluids that contain the components of solid nanosized particles

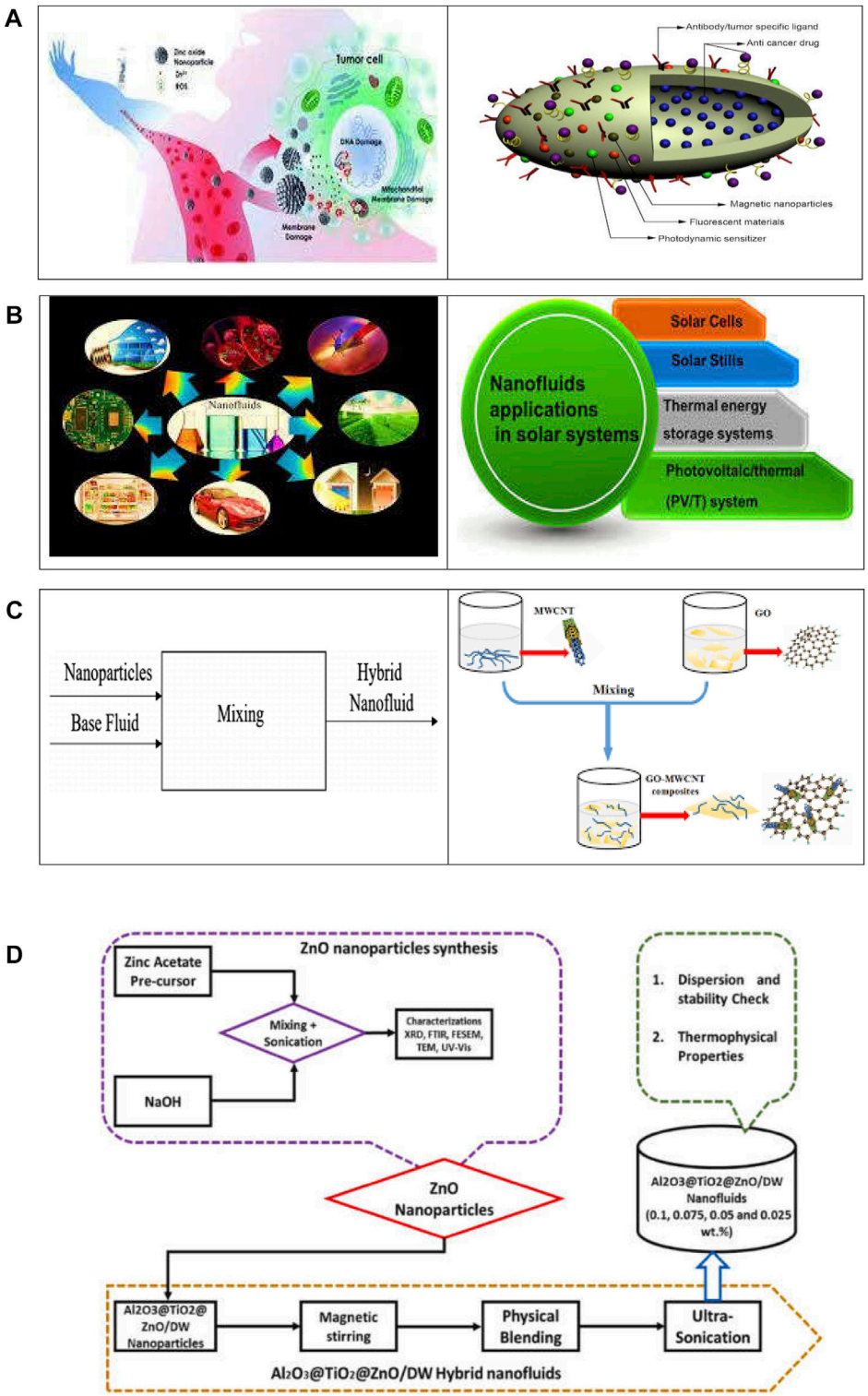

FIGURE 1 | (A) Nanotechnology and the field of biomedical engineering. **(B)**: Applications of nanofluids in different zones. **(C)**: Hybrid nanofluids' synthetization process. **(D)**: Schematic representation of the synthetization process of ternary hybrid nanofluids.

of aforesaid nanomaterials with base solvents such as EO (engine oil), SO (sylthern oil), water, EG (ethylene glycol), and PG (propylene glycol). The addition of these solid components in the base solvents enhances thermal conductivity of the resultant liquids which makes them more effective for nanotechnological purposes.

Nanofluids are extensively utilized for nanotechnological purposes, aerodynamics, paint industries, manufacturing of electronic parts, mechanical engineering, chemical engineering, applied thermal engineering, manufacturing of home appliances, and biomedical engineering. In recent times, biomedical nanotechnologists have directed their attention to induct nanofluids in the field of biomedical engineering. The nanoparticles and nanofluids are utilized to target many diseases in the human body. A milestone that biomedical technologists have achieved is the induction of nanoparticles for targeting cancer cells and tumors in different parts of the human body. More specifically, oxide and silver nanoparticles are used to target the tumor cells. The modern chemotherapy treatment is also based on injecting nanoparticles in human parts to signify the tumor cells (Zhao et al., 2011; Ganau et al., 2018; Khan et al., 2020a; Ray and Bandyopadhyay, 2021). Furthermore, the interaction of nanoparticles with blood as the base solvent is an important research zone in the field of biomedical sciences. **Figure 1A** presents the role of nanoparticles in nanotechnology used in biomedical engineering.

World-renowned researchers did not stop their effects, and they worked on the modifications of nanoparticles and synthesized various nanofluids by combining metallic nanoparticles under various base solvents. They introduced two new classes called hybrid and ternary hybrid nanofluids. Therefore, modern effective heat transport fluids can be characterized in the following three classes:

- Regular liquids such as EG, EO, SO, water, and KS have very restricted applications in nanotechnology because of a very low thermal performance.
- Nanofluids (Zhao et al., 2015; Ahmed et al., 2018; Khan et al., 2018; Ali et al., 2019; Ahmed et al., 2020; Prasad et al., 2020) (1st generation thermal transport fluids) such as Al_2O_3/EG, AA7072/EO, SWCNTs/SO, CNTs/water, and $MgZn_6Zr$/KS have better heat performance and are more suitable for broad uses than regular liquids.
- Hybrid nanofluids (Ilyas et al., 2021; Ijaz, 2021; Mohyud-Din et al., 2020; Imran et al., 2020; Khashi'ie et al., 2022; Said et al., 2021; Khan et al., 2020b) (2nd generation thermal transport fluids) such as MWCNTs-Al_2O_3/EG, AA7075-AA7072/H_2O, magneto-nanofluid (Abbasi et al., 2017 andKhan et al., 2017), MWCNTs-SWCNTs/SO, Ag-$CoFe_3O_4$/water, and $MgZn_6Zr$-$MnZnFe_3O_4$/KS have improved heat transport and are effectively used for different nanotechnology purposes than the preceding two classes of the fluids.
- Tri-hybrid nanofluids (Ramadhan et al., 2019; Muzaidi et al., 2021; Palanisamy et al., 2021; Ramadhan et al., 2021; Hou et al., 2022) (3rd generation of thermal transport fluids; addition of a third nanoparticle (Adnan et al., 2022) in the hybrid nanoparticles) are a very recently developed class and exhibit an ultra-high thermal performance which makes it superior to the preceding three classes of the fluids. In these fluids, two metallic/non-metallic or other nanoparticles are induced in the host solvent to synthesize the resultant tri-hybrid nanofluids [SWCNTs-MWCNTs-Al_2O_3/EG, $MgZn_6Zr$-AA7075-AA7072/EO, MWCNTs-SWCNTs-Ag/SO, $MnZnFe_3O_4$-Ag-$CoFe_3O_4$/water, and $NiZnFe_3O_4$-$MgZn_6Zr$-$MnZnFe_3O_4$/KS]. Induced tri-nanoparticles enhance thermal conductivity at a high level, which improves its heat transport capability.

Figures 1B–D elaborate the applications or the synthetization procedure of nano, hybrid, and ternary hybrid nanofluids which have extensive uses in the modern world.

Recently, Ali et al. (2021) disclosed the influences of 1st order activation energy phenomena on thermal transportation in the nanoliquid known as Oldroyd-B nanofluid. The problem is taken over a UHSPR and handled numerically. The disclosed results revealed that the fluid motion rises due to stronger thickness effects and the thermal performance of the fluid improved by the index parameter. The imperative studies regarding heat transfer in bio-convection Carreau fluid and magnetized Williamson fluids are examined in the studies by Shahid et al. (2022) and Bhatti et al. (2022), respectively. The authors observed fascinating results regarding the dynamics of the fluids under various physical circumstances that would be beneficial for industrial applications.

The significance of thermal transport is one of the paramount ingredients in new innovations in the world of nanotechnology. Therefore, investigation of the heat transport mechanism attracts the world-renowned scientists and engineers. Thus, they knocked the door of the modern world and initiated the analysis of nanofluids under various constraints because the significance of the heat transport study strengthens its roots not only in the industrial and engineering zone but also in biomedical engineering, aerodynamics, chemical and mechanical engineering, etc. (Alqahtani et al., 2020; AdnanKhan et al., 2021). Detection of cancer cells by allowing interaction of oxide nanoparticles with blood as the base solvent is one of the latest milestones achieved by biotechnologists. The most fascinating applications of the nanofluids' heat transfer lies in the solar thermal plates which increases the capability of the plants to store solar energy. Similarly, there exists a lot of potential applications of nanofluids which are of huge interest of the current world. The conducted research convinced us to disclose the answer to the following questions in front of the modern world's scientists and engineers.

- How to enhance the efficiency of the nanofluids?
- What are the impacts of non-linear thermal radiations on the thermal performance of the nanofluids?
- What is the role of suction and stretching parameters on the velocity and temperature behavior of the nanofluids over a 3D surface?
- What is the significance of convective heat condition in thermal enhancement of the nanofluids?

All the aforementioned issues will be addressed in the extended study and hopefully would be beneficial for applied thermal engineering, biomedical engineering, aerodynamics, more specifically in mechanical engineering and many other purposes that use nanotechnology.

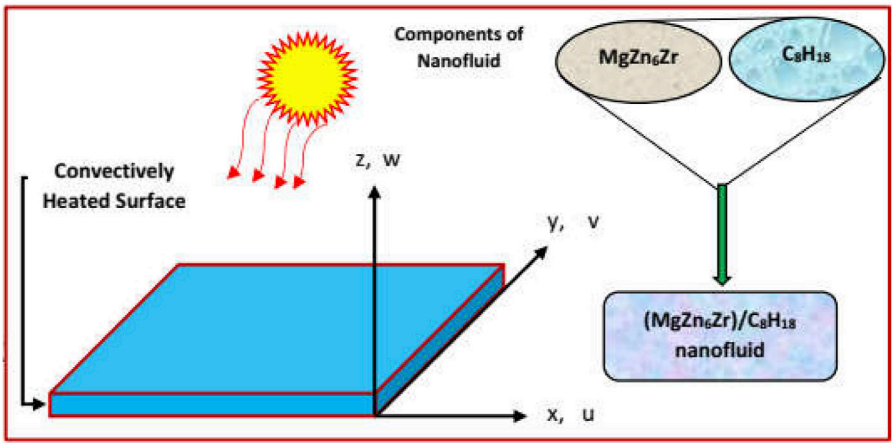

FIGURE 2 | Flow region of $(MgZn_6Zr)/C_8H_{18}$.

MODEL DEVELOPMENT

Model Statement and Geometry

The flow of the $[(MgZn_6Zr)/C_8H_{18}]_{nf}$ steady incompressible nanofluid is configured over a 3D stretchable surface. The velocities are organized as $[\bar{u}, \bar{v}, \bar{w}]^t = [x, y, z]^t$ directions, respectively. The boundaries of the surface are revised *via* first-order velocity slip effects, and the surface is convectively heated. Meanwhile, a uniform suction is also imposed from the surface, and the phenomena of non-linear thermal radiations are induced. The setup of the configured flow over the surface is displayed in **Figure 2**.

In light of the boundary layer approximation theory (BLAT), the flow is constituted by the following mathematical form:

$$\frac{\partial \bar{u}}{\partial x} + \frac{\partial \bar{v}}{\partial y} + \frac{\partial \bar{w}}{\partial z} = 0, \tag{1}$$

$$\bar{u}\frac{\partial \bar{u}}{\partial x} + v\frac{\partial \bar{u}}{\partial y} + w\frac{\partial \bar{u}}{\partial z} = \mathcal{V}_{hnf}\frac{\partial^2 \bar{u}}{\partial z^2}, \tag{2}$$

$$\bar{u}\frac{\partial \bar{v}}{\partial x} + \bar{v}\frac{\partial \bar{v}}{\partial y} + \bar{w}\frac{\partial \bar{u}}{\partial z} = \mathcal{V}_{hnf}\frac{\partial^2 \bar{v}}{\partial z^2}, \tag{3}$$

$$\bar{u}\frac{\partial T}{\partial x} + \bar{v}\frac{\partial T}{\partial y} + \bar{w}\frac{\partial T}{\partial z} = \alpha_{hnf}\frac{\partial^2 T}{\partial Z^2} + \frac{16\sigma^*}{3k^*\left(\rho C p_{hnf}\right)}\left[T^3\frac{\partial T}{\partial z}\right]. \tag{4}$$

With associated BCs, it is expressed as follows:

$$\left\{\begin{array}{c} \bar{u} = ax + \dfrac{(2-\sigma_v)}{\sigma_v}\lambda_o\dfrac{\partial \bar{u}}{\partial z} \\ \bar{v} = by + \dfrac{(2-\sigma_v)}{\sigma_v}\lambda_o\dfrac{\partial \bar{v}}{\partial z} \quad \overline{w} = -\tilde{W} \\ -\dfrac{k_{nf}\partial T}{\partial z} = h\left[T_f - T\right] \end{array}\right\} at\ z = 0$$
$$\bar{u} \to 0\ \ \bar{v} \to 0\ \ T \to T_\infty\ \ as\ \ z \to \infty \tag{5}$$

TABLE 1 | Thermophysical values for the base solvent and nanoparticles.

Nanoparticle/BS	K(W/mk)	Cp (J/kgK)	ρ (kg/m^3)
$MgZn_6Zr$	120	960	2.00
C_8H_{18}	0.145	1868	890

The associated similarity equations are designed as follows:

$$[\bar{u}, \bar{v}, \bar{w}, \eta]^t = \left[F'ax, G'ay, -\sqrt{a\nu_f}\ [F+G], \sqrt{\frac{a}{\nu_f}}z\right]^t. \tag{6}$$

Thermophysical Attributes of Nanofluids

For a particular nanofluid, the following correlations are adopted:

$$\rho_{nf} = \rho_f\mathfrak{R}_1 + \phi\rho_s;\ \ \mu_{nf} = \mu_f * \mathfrak{R}_1^{-\frac{25}{10}},$$
$$\left(\rho C_p\right)_{nf} = \mathfrak{R}_1\left(\rho C_p\right)_f + \phi\left(\rho C_p\right)_s,$$

$$k_{nf}k_f^{-1} = \left[k_s + 2k_f - 2 * \phi\mathfrak{R}_2\right]\Big/\left[k_s + 2k_f + 2 * \phi\mathfrak{R}_2\right].$$

Here; $\mathfrak{R}_1 = (1-\phi)$ and $\mathfrak{R}_2 = (k_f - k_s)$.

Furthermore, the particular values are described in **Table 1** for base solvent engine oil and the nanomaterial:

Final $[(MgZn_6Zr)/C_8H_{18}]_{nf}$ Model

After endorsing the empirical correlations and other related characteristics, the following system is achieved:

$$F''' - \mathfrak{R}_1^{-\frac{25}{10}}\left(\mathfrak{R}_1 + \phi\rho_s/\rho_f\right)\left[\left(F'\right)^2 - (G+F)F''\right] = 0, \tag{7}$$

$$G''' - \mathfrak{R}_1^{-\frac{25}{10}}\left(\mathfrak{R}_1 + \phi\rho_s/\rho_f\right)\left[\left(G'\right)^2 - (G+F)G''\right] = 0, \tag{8}$$

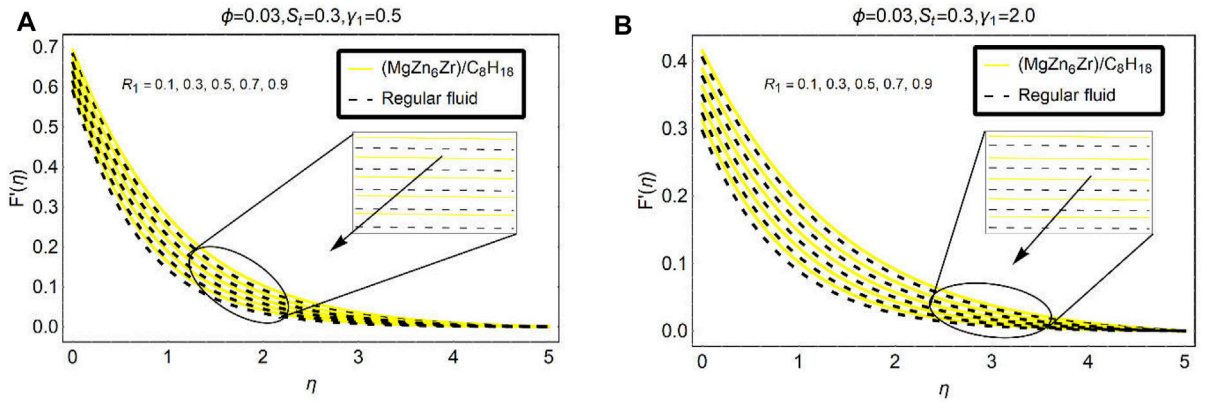

FIGURE 3 | Velocity *via* R_1 for **(A)** γ_1 = 0.5 and **(B)** γ_1 = 2.0.

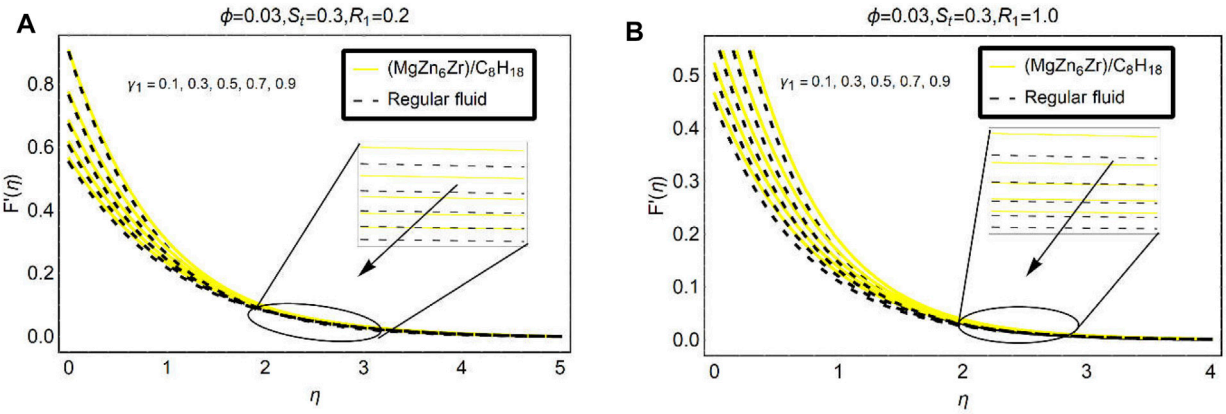

FIGURE 4 | Velocity *via* γ_1 (the slip parameter) for **(A)** R_1 = 0.2 and **(B)** R_1 = 2.0.

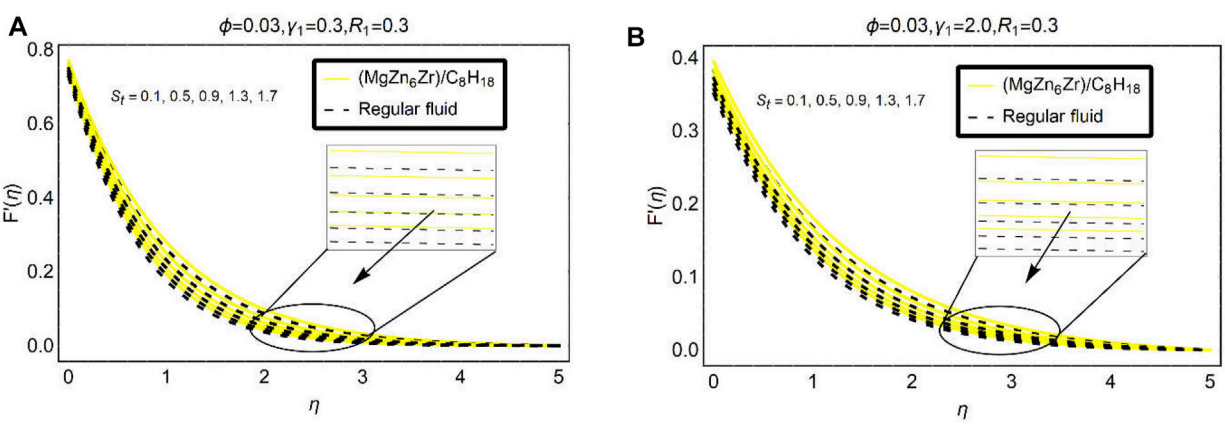

FIGURE 5 | Velocity *via* S_t (the stretching parameter) for **(A)** γ_1 = 0.3 and **(B)** γ_1 = 2.0.

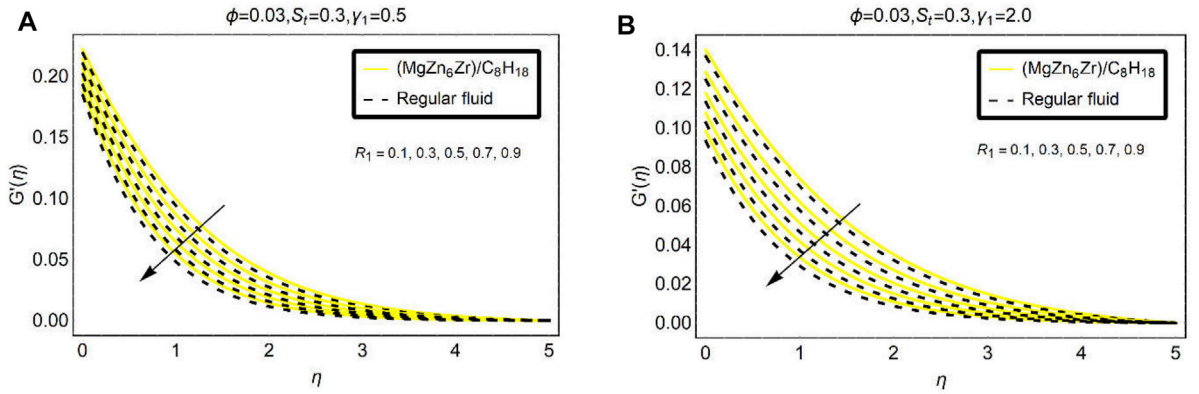

FIGURE 6 | Velocity $G^{'}$ *via* R_1 **(A)** γ_1 = 0.5 and **(B)** γ_1 = 2.0.

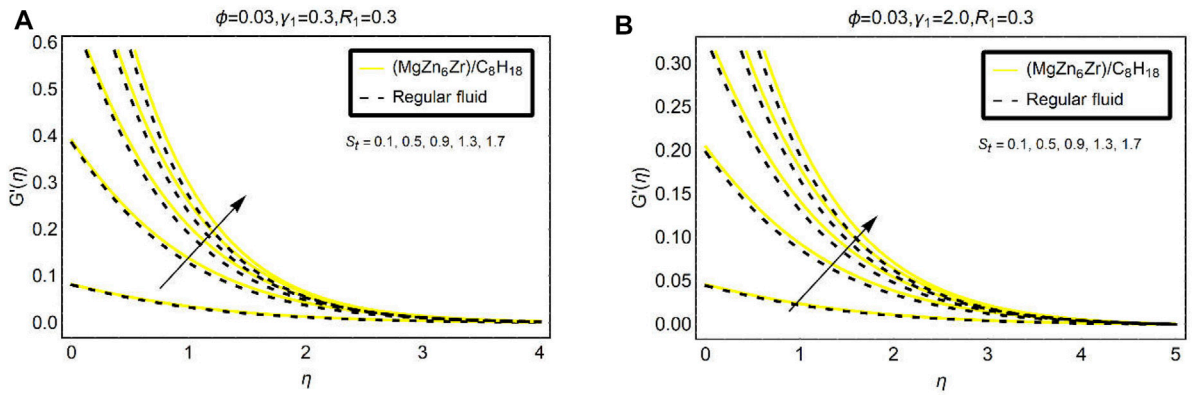

FIGURE 7 | Velocity $G^{'}$ *via* S_t **(A)** γ_1 = 0.3 and **(B)** γ_1 = 2.0.

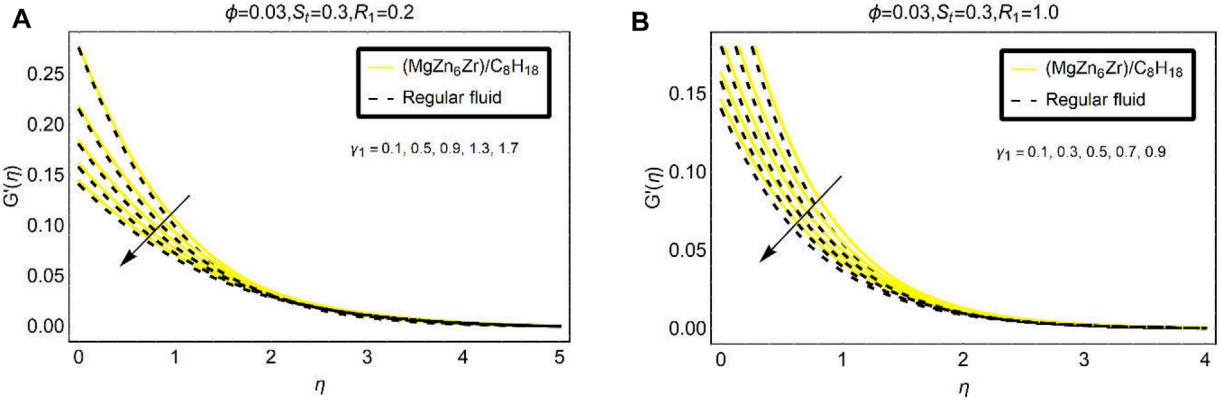

FIGURE 8 | Velocity $G^{'}$ *via* γ_1 **(A)** R_1 = 0.2 and **(B)** R_1 = 1.0.

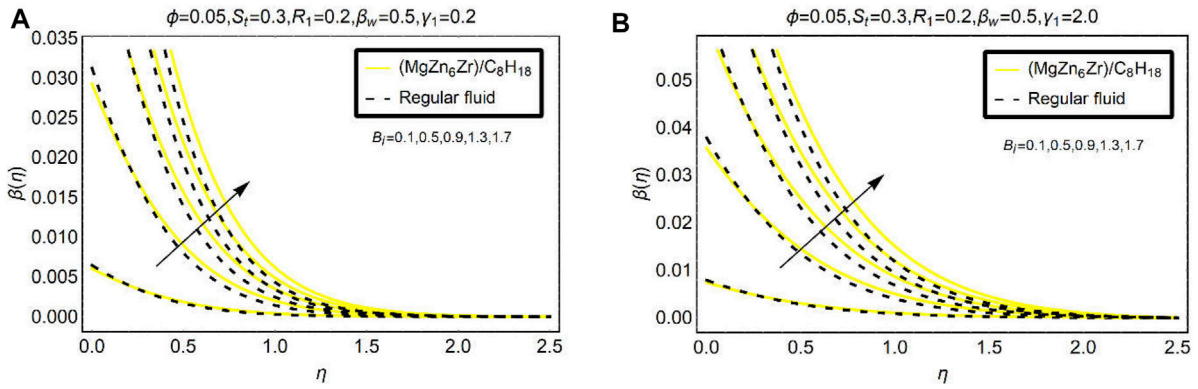

FIGURE 9 | Temperature *via* B_i **(A)** γ_1 = 0.2 and **(B)** γ_1 = 2.0.

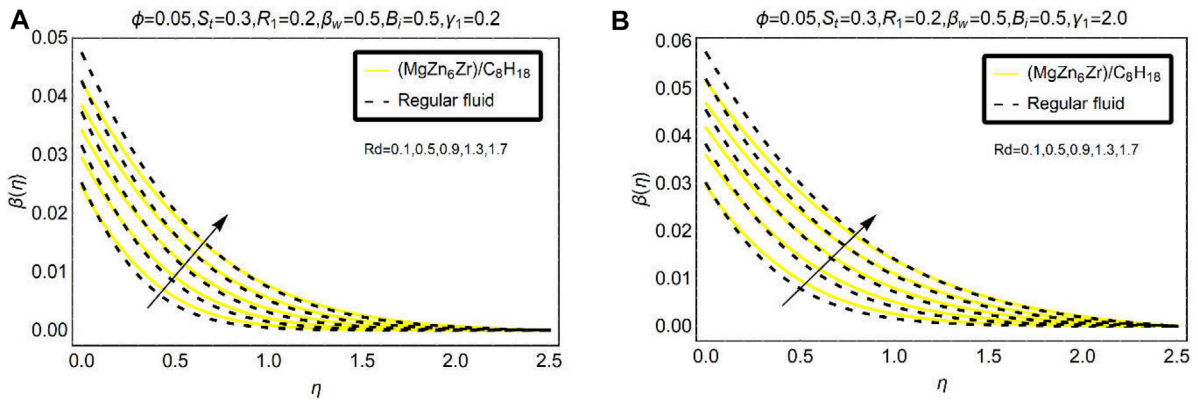

FIGURE 10 | Temperature *via* Rd **(A)** γ_1 = 0.2 and **(B)** γ_1 = 2.0.

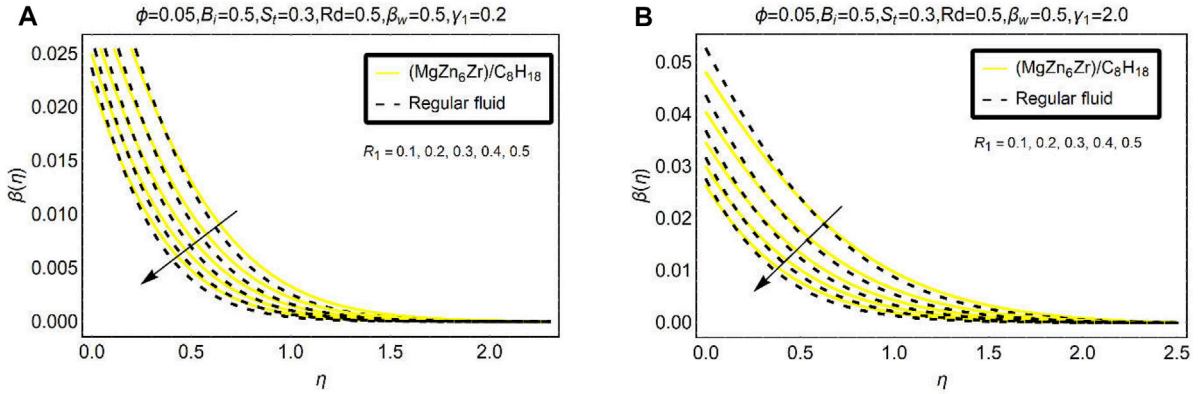

FIGURE 11 | Temperature *via* R_1 **(A)** γ_1 = 0.2 and **(B)** γ_1 = 2.0.

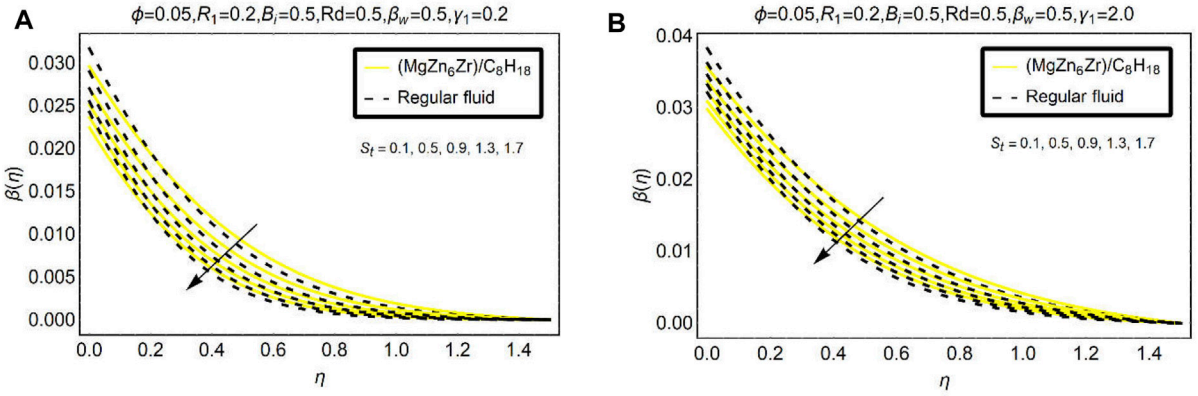

FIGURE 12 | Temperature *via* S_t **(A)** γ_1 = 0.2 and **(B)** γ_1 = 2.0.

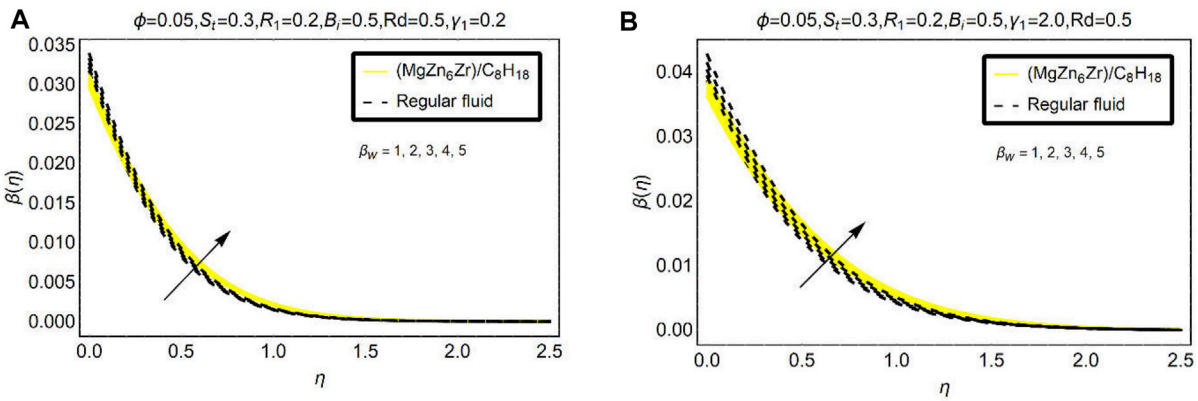

FIGURE 13 | Temperature *via* β_w **(A)** γ_1 = 0.2 and **(B)** γ_1 = 2.0.

$$\frac{1}{\left(\Re_1+\phi\left(\rho C_p\right)_s/\left(\rho C_p\right)_f\right)Pr}\left[\frac{\left[k_s+2k_f-2*\phi\Re_2\right]}{\left[k_s+2k_f+2*\phi\Re_2\right]}+Rd\right]\beta''$$
$$+\frac{Rd}{Pr}\left[\left(\beta_w-1\right)^3\left(3\beta^2\beta'^2+\beta^3\beta''\right)+3\left(\beta_w-1\right)^2\left(2\beta\beta'^2+\beta^2\beta''\right)\right.$$
$$\left.+3\left(\beta_w-1\right)\left(\beta^2+\beta\beta''\right)\right]+\beta'\left(G+F\right)=0. \tag{9}$$

The related BCs are reduced in the following version:

$$\begin{cases} F'(0)=1+\gamma_1F''(0)\quad G'(0)=S_t+\gamma_1G''(0)\quad [F(0)+G(0)]=R_1 \\ \beta^{'(0)}=-\dfrac{k_f}{k_{nf}}\left[B_i\left[1-\beta(0)\right]\right] \\ F'(\infty)\to 0\quad G'(\infty)\to 0\quad \beta(\infty)\to 0. \end{cases} \tag{10}$$

The physical constraints appearing in the model are $S_t = b/a$ (the stretching parameter) and $Rd = 16\sigma^*T_\infty^3/3k^*k_f$, which is the radiation parameter; $B_i = h/k_f\left[\nu_f a^{-1}\right]^{0.5}$ represents the Biot parameter, and $\gamma_1 = \frac{(2-\sigma_v)}{\sigma_v}\lambda_o\sqrt{a\nu_f^{-1}\lambda_0}$ represents the slip parameter.

Furthermore, trends of shear drags are estimated through the following expressions:

$$R_{ex}^{0.5}C_{fx}=\Re_1^{-25/10}F''(0),\ R_{ex}^{0.5}C_{fy}=\Re_1^{-25/10}G''(0).$$

MATHEMATICAL ANALYSIS OF $[(MGZN_6ZR)/C_8H_{18}]_{NF}$

The resultant nanofluid model $[(MgZn_6Zr)/C_8H18]_{nf}$ is tedious in nature and almost impossible to solve it explicitly for a closed form solution. Therefore, the numerical algorithm is applied which works as described subsequently:

- First, the model is written in its appropriate form.
- Substitutions are made, according to the order of the model.

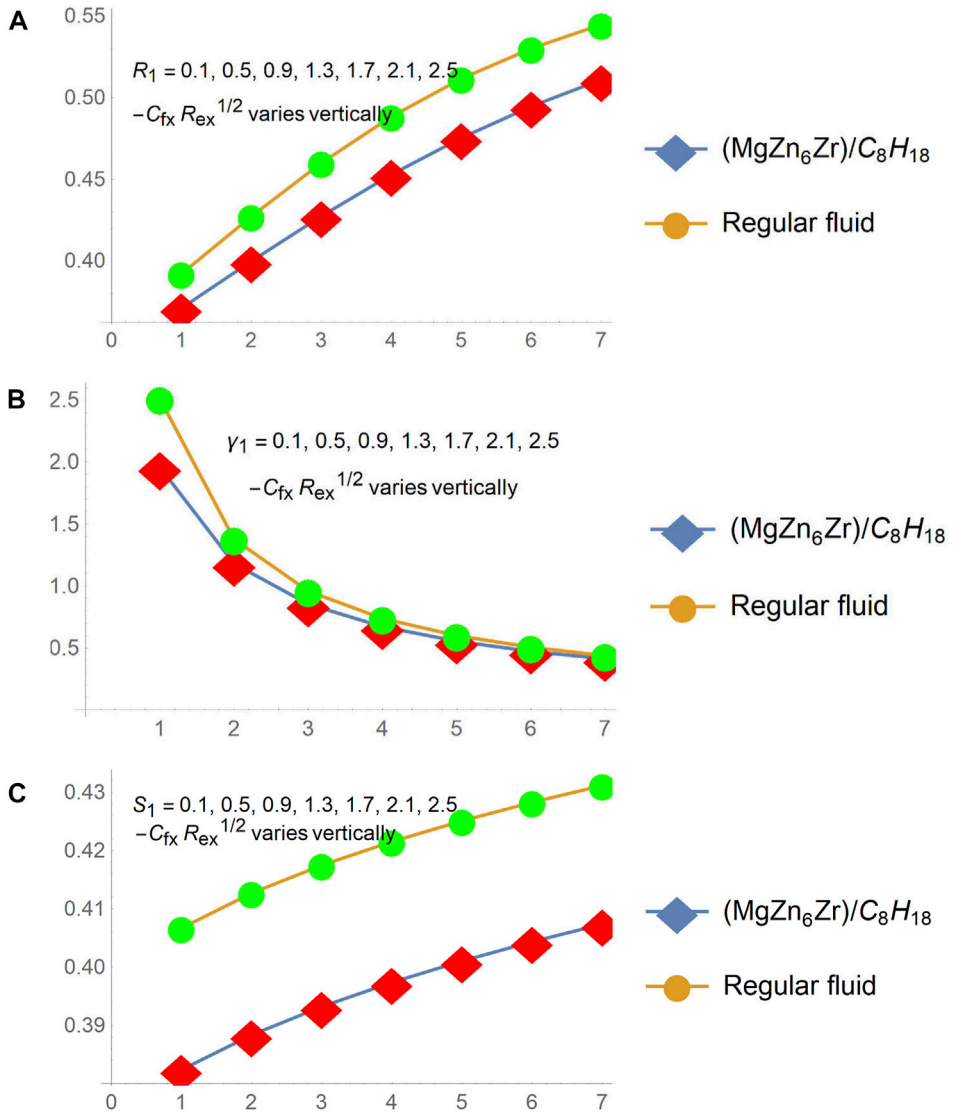

FIGURE 14 | Skin friction *via* **(A)** R_1 **(B)** γ_1 and **(C)** S_t.

- Using those substitutions, the higher order model should be transformed into first order IVP.
- The BCs are adjusted accordingly, and the conditions are set equal to unknowns which will be determined later.
- Finally, the code is allowed to run, and the results are plotted for various physical constraints.

$$F''' = \mathfrak{R}_1^{-\frac{25}{10}}\left(\mathfrak{R}_1 + \phi\rho_s/\rho_f\right)\left[\left(F'\right)^2 - (G+F)F''\right], \quad (11)$$

$$G''' = \mathfrak{R}_1^{-\frac{25}{10}}\left(\mathfrak{R}_1 + \phi\rho_s/\rho_f\right)\left[\left(G'\right)^2 - (G+F)G''\right], \quad (12)$$

$$\beta'' = -\frac{1}{\frac{1}{\left(\mathfrak{R}_1+\phi\left(\rho C_p\right)_s/\left(\rho C_p\right)_f\right)Pr}\left[\frac{\left[k_s+2k_f-2*\phi\mathfrak{R}_2\right]}{\left[k_s+2k_f+2*\phi\mathfrak{R}_2\right]}+Rd\right]}\Bigg[+ \frac{Rd}{Pr}\left[\left(\beta_w-1\right)^3\left(3\beta^2\beta'^2+\beta^3\beta''\right)+3\left(\beta_w-1\right)^2\left(2\beta\beta'^2 + \beta^2\beta''\right)+3\left(\beta_w-1\right)\left(\beta^2+\beta\beta''\right)\right]+\beta'\left(G+F\right)\Bigg]. \quad (13)$$

Now, the following transformations are assigned:

$$\left[\tilde{\mathfrak{1}}_1 \quad \tilde{\mathfrak{1}}_2 \quad \tilde{\mathfrak{1}}_3 \quad \tilde{\mathfrak{1}}_3'\right]^t = \left[F \quad F' \quad F'' \quad F'''\right]^t,$$

$$\left[\tilde{\mathfrak{1}}_4 \quad \tilde{\mathfrak{1}}_5 \quad \tilde{\mathfrak{1}}_6 \quad \tilde{\mathfrak{1}}_6'\right]^t = \left[G \quad G' \quad G'' \quad G'''\right]^t,$$

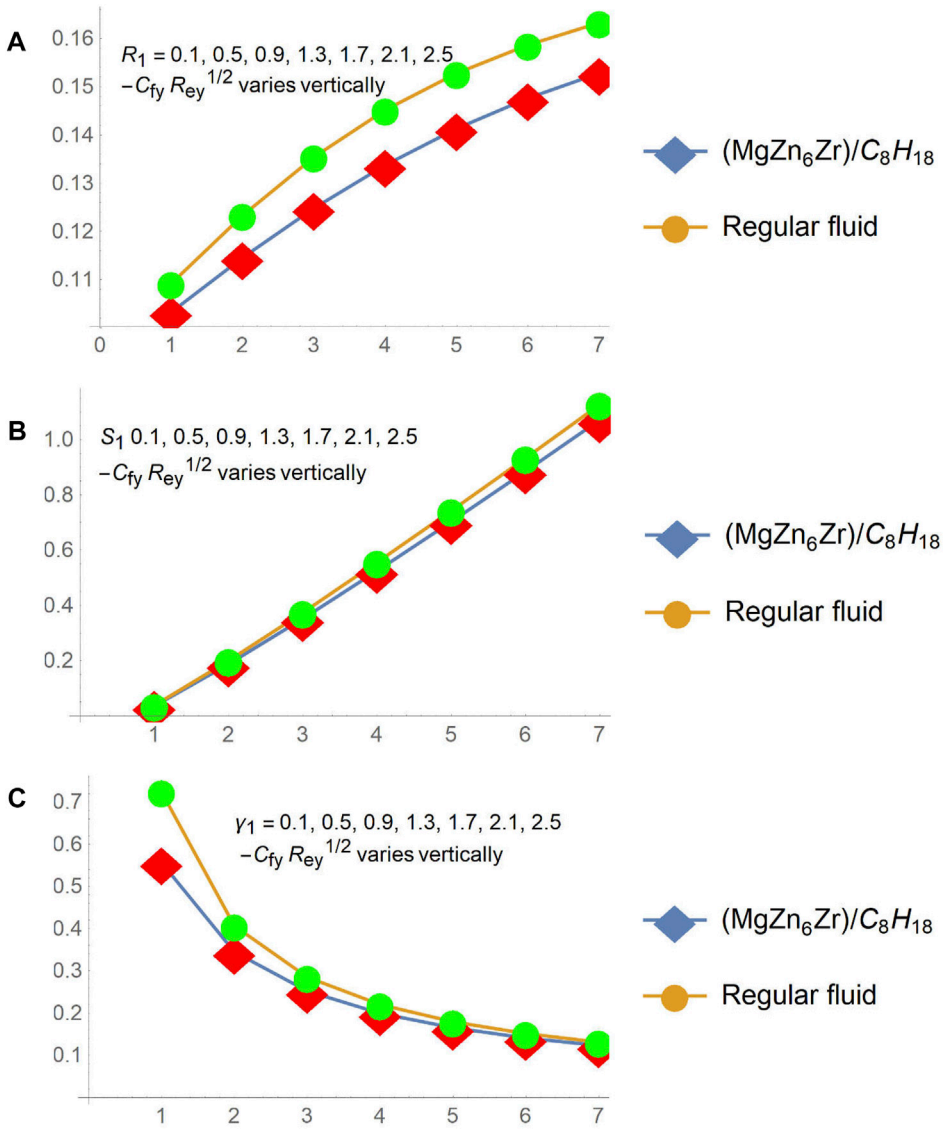

FIGURE 15 | Skin friction in *y*-direction *via* **(A)** R_1 **(B)** S_t and **(C)** γ_1.

$$\left[\tilde{\mathfrak{T}}_7 \;\; \tilde{\mathfrak{T}}_8 \;\; \tilde{\mathfrak{T}}_8'\right]^t = \left[\beta \;\; \beta' \;\; \beta''\right]^t,$$

Utilization of the aforementioned transformations leads to the following version of the model:

$$\tilde{\mathfrak{T}}_3' = \mathfrak{R}_1^{-\frac{25}{10}}\left(\mathfrak{R}_1 + \phi\rho_s/\rho_f\right)\left[\left(\tilde{\mathfrak{T}}_2'\right)^2 - \left(\tilde{\mathfrak{T}}_4 + \tilde{\mathfrak{T}}_1\right)\tilde{\mathfrak{T}}_3\right],$$

$$\tilde{\mathfrak{T}}_6' = \mathfrak{R}_1^{-\frac{25}{10}}\left(\mathfrak{R}_1 + \phi\rho_s/\rho_f\right)\left[\left(\tilde{\mathfrak{T}}_5'\right)^2 - \left(\tilde{\mathfrak{T}}_4 + \tilde{\mathfrak{T}}_1\right)\tilde{\mathfrak{T}}_6\right],$$

$$\tilde{\mathfrak{T}}_8' = -\frac{1}{\frac{1}{\left(\mathfrak{R}_1+\phi\left(\rho C_p\right)_s/\left(\rho C_p\right)_f\right)Pr}\left[\frac{\left[k_s+2k_f-2*\phi\mathfrak{R}_2\right]}{\left[k_s+2k_f+2*\phi\mathfrak{R}_2\right]} + Rd\right]}$$
$$\left[+\frac{Rd}{Pr}\left[\left(\beta_w-1\right)^3\left(3\tilde{\mathfrak{T}}_7^2\tilde{\mathfrak{T}}_8'^2 + \tilde{\mathfrak{T}}_7^3\tilde{\mathfrak{T}}_8''\right) + 3\left(\beta_w-1\right)^2\left(2\tilde{\mathfrak{T}}_7\tilde{\mathfrak{T}}_8'^2 + \tilde{\mathfrak{T}}_7^2\tilde{\mathfrak{T}}_8''\right) + 3\left(\beta_w-1\right)\left(\tilde{\mathfrak{T}}_7^2 + \tilde{\mathfrak{T}}_7\tilde{\mathfrak{T}}_8''\right)\right] + \tilde{\mathfrak{T}}_8\left(\tilde{\mathfrak{T}}_4 + \tilde{\mathfrak{T}}_1\right)\right].$$

Thereafter, the code is executed for the results.

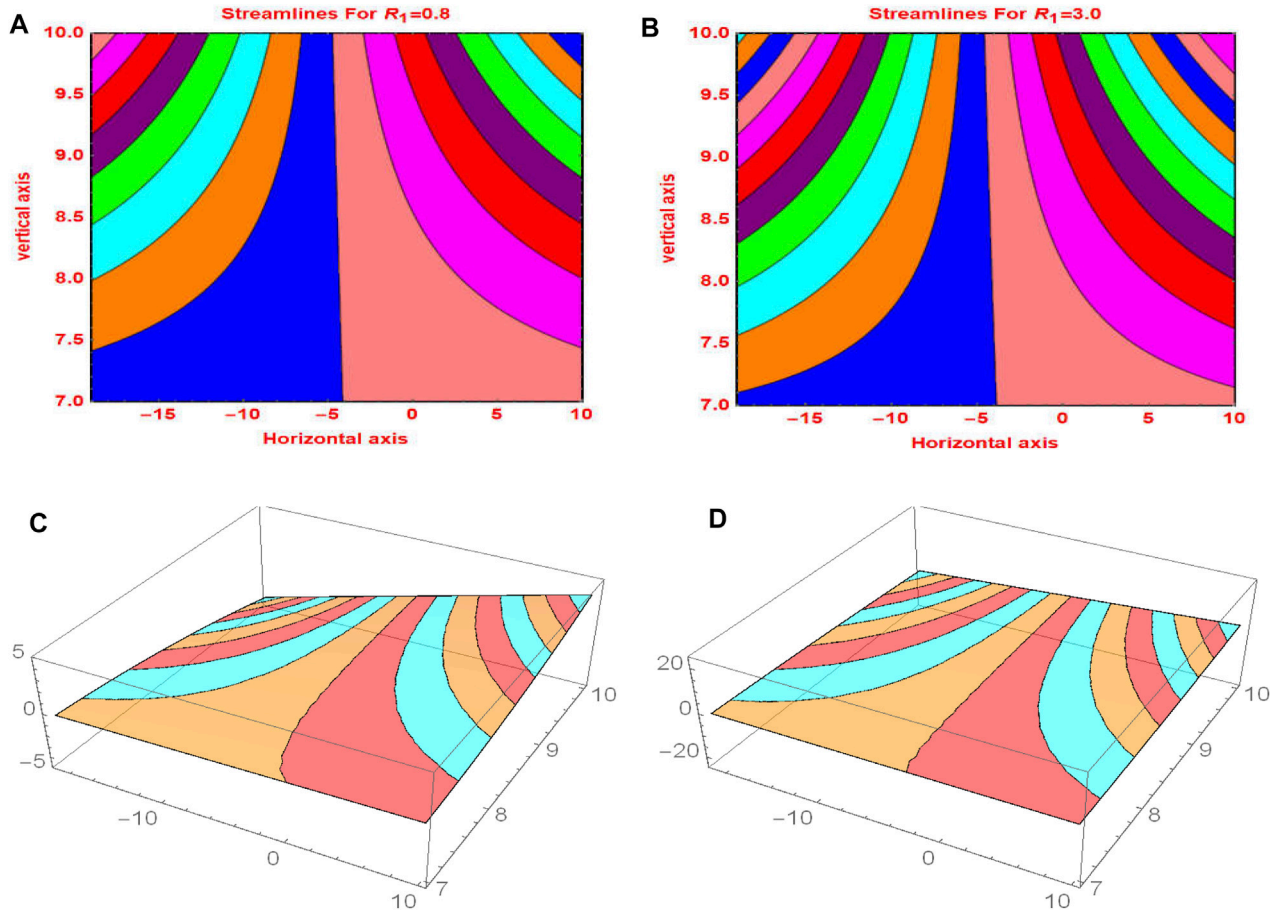

FIGURE 16 | Streamlines *via* **(A)** R_1 = 0.8, **(B)** R_1 = 3.0, **(C)** 3D for R_1 = 0.8, and **(D)** 3D for R_1 = 3.0.

RESULTS AND DISCUSSION AGAINST THE PHYSICAL CONSTRAINTS

The velocities (F', G'), temperature, and skin friction coefficient under the impact of various physical constraints such as S_t (the stretching parameter), γ_1 (the slip parameter), R_1 (the suction parameter), B_i (the Biot parameter), and Rd (thermal radiation) are provided in the subsequent subsections.

The Velocity F′ of $[(MgZn_6Zr)/C_8H_{18}]_{nf}$

The influences of suction, velocity slip, and stretching parameter on the velocity F' of $[(MgZn_6Zr)/C_8H_{18}]_{nf}$ over the desired region are displayed in **Figures 3–5**, respectively. The velocity drops by strengthening the suction effects from the surface. Physically, when the fluid sucks from the surface, more fluid particles are attracted toward the surface. Consequently, attachment of the particles to the surface upsurges due to which the motion drops. The motion of the fluid layers adjacent to the surface abruptly declines due to the dominant effects of suction. Furthermore, the velocity from the surface to the free stream decays rapidly when γ_1 = 0.5 is fixed. However, this region increases by assigning the slip parameter value, i.e., γ_1 = 2.0. In the surroundings of the surface, the velocity decays promptly because of stronger R_1 influences. This behavior of the velocity gradient $F^{'}$ is elucidated in **Figure 3**.

The slip parameter effects on $F^{'}$ are showed in **Figure 4**. **Figure 4A** depicts the behaviour of velocity profile against varying γ_1. The analysis of the results reveals that the velocity significantly changes for higher slip effects. The asymptotic velocity region decreases for R_1 = 0.2, and the velocity obeys the free streamflow condition almost after $\eta > 2.0$. Another view of the fluid motion for various γ_1 and R_1 = 2.0 is depicted in **Figure 4B**. Observation from the results reveals that this time, maximum decrement in F' occurs because the suction parameter rises from 0.2 to 1.0. Physically, the particles are stuck with the surface. The fluid layer in the surroundings of the surface has an optimum decreasing behavior, whereas it becomes minimum for successive layers as the friction declines between those layers which allow the particles to move freely.

The stretching effects (S_t) on the velocity gradient F' are pictured in **Figure 5**. The gradient of velocity drops for a more stretchable surface. Physically, the stretching surface enlarges the flow region, and the particles spread over the surface in both directions. Due to enlargement in the surface area, the velocity gradient reduces. However, quite a rapid decrement is noticed when γ_1 is fixed at 2.0.

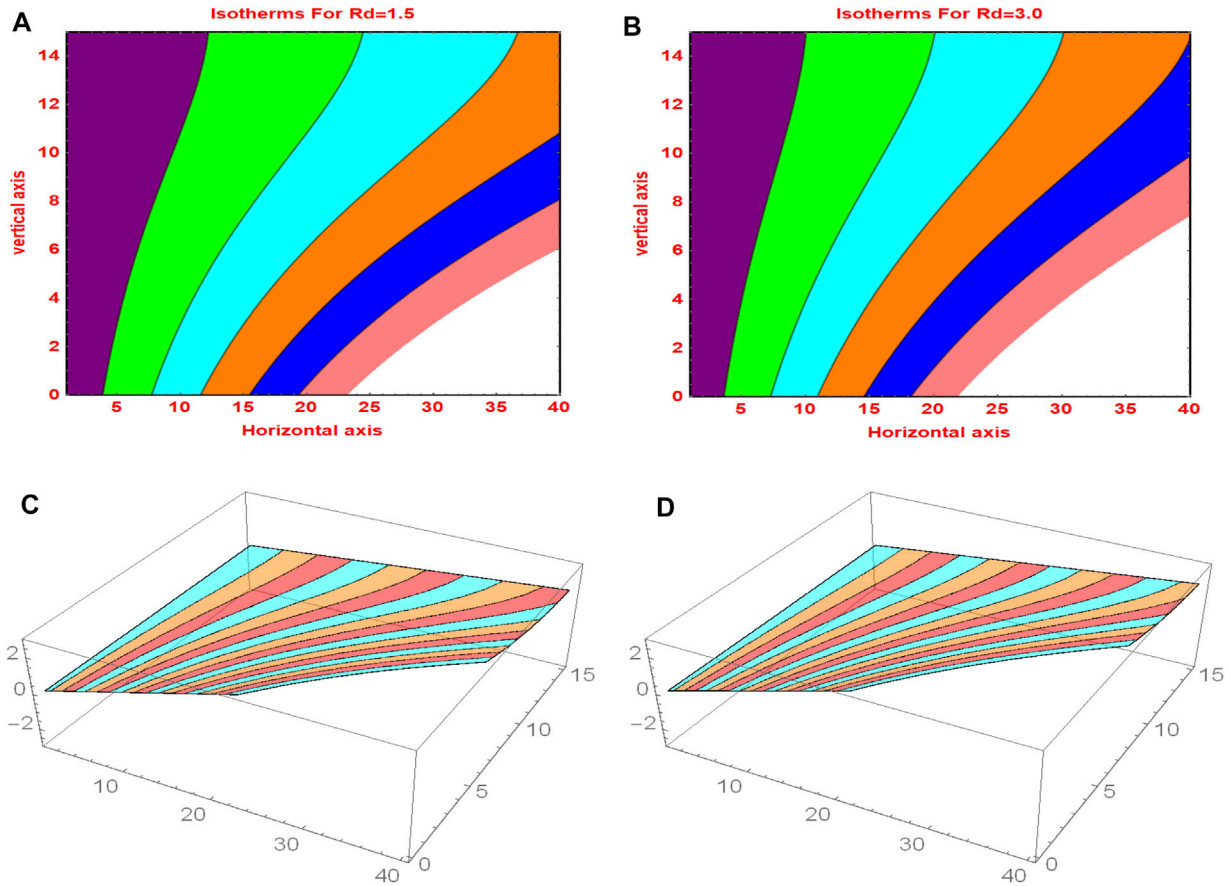

FIGURE 17 | Isotherms *via* **(A)** *Rd* = 1.5, **(B)** *Rd* = 3.0, **(C)** 3D for *Rd* = 1.5, and **(D)** 3D for *Rd* = 3.0.

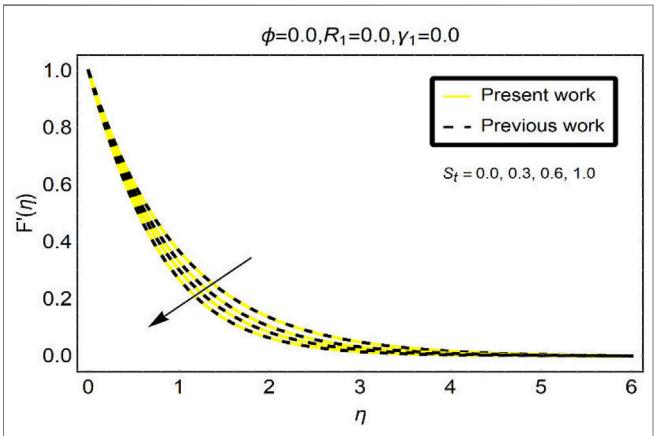

FIGURE 18 | Authentication of the study with a previously reported study.

The Velocity G′ of $[(MgZn_6Zr)/C_8H_{18}]_{nf}$

Figures 6–8 explain to analyze the behavior velocity gradient G' of $[(MgZn_6Zr)/C_8H_{18}]_{nf}$ over a 3D stretchable surface. The results are plotted for R_1, S_t , and γ_1 in **Figures 6–8**, respectively.

The suction parameter opposes the fluid motion $G^{'}$ over the surface. The fluid particles along the *y*-direction are also dragged at the surface due to constant suction. The attraction of particles at the surface is a dominant characteristic of the suction phenomena. Therefore, more particles transform in the surroundings of the surface. The fluid layer very near to the surface moves very slowly due to suction, and the extra existence of friction between the surface and adjacent layer opposes its motion. Thus, the frictional phenomena reduce far from the surface, and the friction between the successive layers decreases; therefore, its fluid velocity drops slowly. It is also noticed that when slip effects change from 0.5 to 2.0, optimum declines in the velocity occur. All these effects are discussed in **Figure 6**.

Very fascinating trends in the velocity gradient $G^{'}$ against higher S_t (stretching effects) are elaborated in **Figure 7**. The stretching parameter boosts the velocity gradient $G^{'}$ abruptly. More significant changes occur by increasing the stretching parameter. The particles stuck with the surface gain extra momentum due to the sudden stretching of the surface. Therefore, the velocity rises prominently for higher S_t. Considering the concerns of the ambient position of the surface, the velocity decays and follows the ambient flow conditions.

Figure 8 is associated with the variations in $G^{'}$ for various values of the slippery parameter γ_1. The parameter opposes the velocity $G^{'}$ in the existence of suction (R_1) and stretching (S_t). The

velocity behavior decreases for a more slippery surface, and maximum changes were noticed when suction effects changed from 0.2 (**Figure 8A**) to 1.0 (**Figure 8B**). Thus, it is observed that the velocity can be controlled by reducing suction from the surface.

Thermal Behavior of $[(MgZn_6Zr)/C_8H_{18}]_{nf}$

Figure 9 elucidates the temperature enhancement in $[(MgZn_6Zr)/C_8H_{18}]_{nf}$ for various convectively heated surface values. From the results' inspection, it discloses that the temperature enhances by increasing surface convection. The imposed heat convection condition at the surface contributes to the energy transfer. Physically, the applied convection condition transfers energy to the neighboring particles at the surface. When these particles gain energy to some extent, these provide the energy to the next particles. In a similar way, the fluid temperature enlarges. In the surface surroundings, these effects are dominant due to stronger convection. The temperature vanishes ambiently for $\gamma_1 = 0.2$,while for a more slippery surface ($\gamma_1 = 2.0$), the ambient position enlarges.

Thermal radiation is an imperative physical phenomenon to improve thermal efficiency of the nanofluids and regular liquids to some limit. Thermal radiations in the existence of the convective heat condition imperatively contribute to thermal enhancement of the nanofluid. Imposed thermal radiations provide energy to the fluid particles that upsurge the ability of the temperature. High thermal radiations are a better heat transport source in the study of nanofluids. Furthermore, high thermal conductance of the nanofluid plays an important role in the energy transport. These effects are displayed in **Figure 10**.

Figures 11 and **12** highlight the temperature variations for suction and stretching effects, respectively. It is inspected that temperature $\beta(\eta)$ drops for both suction and S_t. Physically, collision between the particles declines, and when the fluid particles become more compact due to a stronger suction near the surface, temperature drops. Asymptotic behavior of the temperature occurs far from the surface (free stream position). On the other hand, temperature behavior against stretching effects is shown in **Figure 12**. This time, temperature reduces quite slowly than suction variations. **Figure 13** discloses that temperature of $[(MgZn_6Zr)/C_8H_{18}]_{nf}$ rises for the increasing temperature ratio parameter β_w. The temperature rises very slowly, and finally, it obeys the ambient temperature condition.

Skin Friction, Streamlines, and Isotherms

Figures 14 and **15** present the shear stress trends along both directions ($-C_{fx}R_{ex}$ and $-C_{fy}R_{ey}$), against suction (R_1), slip (γ_1), and stretching (S_t) effects, respectively. From **Figure 14** to **Figure 15**, decrement in the shear stresses (along both directions) is noticed for a stronger slippery surface. However, shear stresses upsurge for suction and stretching parameters. Maximum increment occurs for ($-C_{fx}R_{ex}$). An interesting pattern for streamlines and isotherms against the pertinent parameters is elucidated in **Figure 16** and **Figure 17**, respectively.

Reliability of the Study

This subsection is organized to align the conducted study with previously reported work. Therefore, a graphical comparison is provided by restricting the involved physical constraints ($\phi = 0.0$, $R_1 = 0.0$, $\gamma_1 = 0.0$) with the published work of Devi et al. (Devi and Devi, 2016) with $M = 0$. It is realized that the velocity curves of the present work under restricted parametric values coincide with the existing work which provide the study's reliability. Comparative analysis is depicted in **Figure 18** for varying S_t

CONCLUSION

A study of $[(MgZn_6Zr)/C_8H_{18}]_{nf}$ was conducted over a three-dimensional surface by encountering the influences of thermal radiations and the convective heat condition. The boundaries of the surface are modified with velocity slip, suction, and stretching effects. The governing flow model of $[(MgZn_6Zr)/C_8H_{18}]_{nf}$ is solved numerically, and the results are provided against the physical constraints. From the study, it is summarized that

- The velocities of $[(MgZn_6Zr)/C_8H_{18}]_{nf}$ reduce by strengthening suction (R_1) and slip (γ_1) parameters.
- The velocity G' significantly rises for the stretching parameter, and more significant changes occur at the surface.
- The convective heat condition provides extra energy to the fluid particles from the surface which enhanced $[(MgZn_6Zr)/C_8H_{18}]_{nf}$ temperature.
- Thermal radiations are also significantly contributed for thermal enhancement in $[(MgZn_6Zr)/C_8H_{18}]_{nf}$.
- The study of $[(MgZn_6Zr)/C_8H_{18}]_{nf}$ will be more effective in applied thermal engineering and heat transport problems in the modern world.

DATA AVAILABILITY STATEMENT

The study was based on numerical computations and data required for the study. The raw data supporting the conclusion of this article will be made available by the authors, without undue reservation.

AUTHOR CONTRIBUTIONS

Adnan and UK investigated the research gap and performed mathematical modeling; Adnan and UK wrote the original draft; NA and IK coded the model and methodology; Adnan, NA and IK contributed to results and discussion; AM and SM validated the study; Adnan, AM and SM revised the manuscript.

REFERENCES

Abbasi, A., Ahmed, N., and Mohyud-Din, S. T. (2017). Flow of Magneto-Nanofluid over a Thermally Stratified Bi-directional Stretching Sheet in the Presence of Ohmic Heating: A Numerical Study of Particle Shapes. *Eng. Computations* 34 (8), 2499–2513.

Adnan, W. A., Alghtani, A. H., Khan, I., and Andualem, M. (2022). Thermal Transport in Radiative Nanofluids by Considering the Influence of Convective Heat Condition. *J. Nanomater.* 2022, 1854381. doi:10.1155/2022/1854381

AdnanKhan, U., KhanMohyud-Din, U. S. T., Ahmed, N. D. B., Tauseef Mohyud-Din, S., Khan, I., Baleanu, D., et al. (2021). Al2O3 and γAl2O3 Nanomaterials Based Nanofluid Models with Surface Diffusion: Applications for Thermal Performance in Multiple Engineering Systems and Industries. *CMC-Computers Mater. Continua* 66 (2), 1563–1576. doi:10.32604/cmc.2020.012326

Ahmed, N., Abbasi, A., Saba, F., Khan, U., and Mohyud-Din, S. T. (2018). Flow of Ferro-Magnetic Nanoparticles in a Rotating System: a Numerical Investigation of Particle Shapes. *Indian J. Phys.* 92, 969–977. doi:10.1007/s12648-018-1186-4

Ahmed, N., AdnanKhan, U., Mohyud-Din, S. T., Khan, I., Hussain, R. I., et al. (2020). A Novel Investigation and Hidden Effects of MHD and Thermal Radiations in Viscous Dissipative Nanofluid Flow Models. *Front. Phys.* 8. doi:10.3389/fphy.2020.00075

Ali, A., Shehzadi, K., Sulaiman, M., and Asghar, S. (2019). Heat and Mass Transfer Analysis of 3D Maxwell Nanofluid over an Exponentially Stretching Surface. *Phys. Scr.* 94 (6), 065206. doi:10.1088/1402-4896/ab07cf

Ali, Z., Zeeshan, A., Bhatti, M. M., Hobiny, A., and Saeed, T. (2021). Insight into the Dynamics of Oldroyd-B Fluid over an Upper Horizontal Surface of a Paraboloid of Revolution Subject to Chemical Reaction Dependent on the First-Order Activation Energy. *Arab J. Sci. Eng.* 46, 6039–6048. doi:10.1007/s13369-020-05324-6

Alqahtani, A. M., AdnanKhan, U., Ahmed, N., Mohyud-Din, S. T., and Khan, I. (2020). Numerical Investigation of Heat and Mass Transport in the Flow over a Magnetized Wedge by Incorporating the Effects of Cross-Diffusion Gradients: Applications in Multiple Engineering Systems. *Math. Probl. Eng.* 2020, 2475831. doi:10.1155/2020/2475831

Bhatti, M. M., Arain, M. B., Zeeshan, A., Ellahi, R., and Doranehgard, M. H. (2022). Swimming of Gyrotactic Microorganism in MHD Williamson Nanofluid Flow between Rotating Circular Plates Embedded in Porous Medium: Application of thermal Energy Storage. *J. Energ. Storage* 45, 103511. doi:10.1016/j.est.2021.103511

Devi, S. S. U., and Devi, S. P. A. (2016). Numerical Investigation of Three-Dimensional Hybrid Cu-Al2O3/water Nanofluid Flow over a Stretching Sheet with Effecting Lorentz Force Subject to Newtonian Heating. *Can. J. Phys.* 94, 490–496. doi:10.1139/cjp-2015-0799

Ganau, M., Paris, M., Syrmos, N., Ganau, L., Ligarotti, G., Moghaddamjou, A., et al. (2018). How Nanotechnology and Biomedical Engineering Are Supporting the Identification of Predictive Biomarkers in Neuro-Oncology. *Medicines* 5, 23. doi:10.3390/medicines5010023

Hou, E., Wang, F., Nazir, U., Sohail, M., Jabbar, N., and Thounthong, P. (2022). Dynamics of Tri-hybrid Nanoparticles in the Rheology of Pseudo-plastic Liquid with Dufour and Soret Effects. *Micromachines* 13, 201. doi:10.3390/mi13020201

Ijaz, M. (2021). Transportation of Hybrid Nanoparticles in Forced Convective Darcy-Forchheimer Flow by a Rotating Disk. *Int. Commun. Heat Mass Transfer* 122 (ID), 105177.

Ilyas, H., Ahmad, I., Raja, M. A. Z., Tahir, M. B., and Shoaib, M. (2021). Neuro-intelligent Mappings of Hybrid Hydro-Nanofluid Al2O3-Cu-H2o Model in Porous Medium over Rotating Disk with Viscous Dissolution and Joule Heating. *Int. J. Hydrogen Energ.* 46 (55), 28298–28326. doi:10.1016/j.ijhydene.2021.06.065

Imran, A., Akhtar, R., Zhiyu, Z., Shoaib, M., and Raja, M. A. Z. (2020). Heat Transfer Analysis of Biological Nanofluid Flow through Ductus Efferentes. *AIP Adv.* 10, 035029. doi:10.1063/1.5135298

Khan, A. S., Nie, Y., Shah, Z., Dawar, A., Khan, W., and Islam, S. (2018). Three-Dimensional Nanofluid Flow with Heat and Mass Transfer Analysis over a Linear Stretching Surface with Convective Boundary Conditions. *Appl. Sci.* 8, 2244. doi:10.3390/app8112244

Khan, U., Abbasi, A., Ahmed, N., and Mohyud-Din, S. T. (2017). Particle Shape, thermal Radiations, Viscous Dissipation and Joule Heating Effects on Flow of Magneto-Nanofluid in a Rotating System. *Ec* 34 (8), 2479–2498. doi:10.1108/ec-04-2017-0149

Khan, U. A., AdnanAhmed, N., Mohyud-Din, S. T., Baleanu, D., Khan, I., et al. (2020). A Novel Hybrid Model for Cu-Al2O3/H2O Nanofluid Flow and Heat Transfer in Convergent/Divergent Channels. *Energies* 13, 1686–1687. doi:10.3390/en13071686

Khan, U. A., AdnanAhmed, N., Mohyud-Din, S. T., Chu, Y.-M., Khan, I., et al. (2020). γ-Nanofluid Thermal Transport between Parallel Plates Suspended by Micro-cantilever Sensor by Incorporating the Effective Prandtl Model: Applications to Biological and Medical Sciences. *Molecules* 25, 1777. 8. doi:10.3390/molecules25081777,

Khashi'ie, N. S., Arifin, N. M., Rosca, N. C., Rosca, A. V., and Pop, I. (2022). Three-dimensional Flow of Radiative Hybrid Nanofluid Past a Permeable Stretching/shrinking Sheet with Homogeneous-Heterogeneous Reaction. *Hff* 32 (2), 568–588. doi:10.1108/hff-01-2021-0017

Mohyud-Din, S. T., Adnan Khan, U., Ahmed, N., Khan, I., Abdeljawad, T., et al. (2020). Thermal Transport Investigation in Magneto-Radiative GO-MoS2/H2O-C2h6o2 Hybrid Nanofluid Subject to Cattaneo-Christov Model. *Molecules* 25, 2592. doi:10.3390/molecules25112592

Muzaidi, N. A. S., Fikri, M. A., Wong, K. N. S. W. S., Sofi, A. Z. M., Mamat, R., Adenam, N. M., et al. (2021). Heat Absorption Properties of CuO/TiO2/SiO2 Trihybrid Nanofluids and its Potential Future Direction towards Solar thermal Applications. *Arabian J. Chem.* 14 (4), 103059. doi:10.1016/j.arabjc.2021.103059

Palanisamy, R., Parthipan, G., and Palanic, S. (2021). Study of Synthesis, Characterization and Thermo Physical Properties of Al2O3-SiO2-TiO2/H2O Base Tri-hybrid Nanofluid. *Dig. J. Nanomater. Biostructures* 16 (3), 939–949.

Prasad, K. V., Vaidya, H., Vajravelu, K., Manjunatha, G., Rahimi-Gorji, M., and Basha, H. (2020). Heat Transfer Analysis of Three-Dimensional Mixed Convective Flow of an Oldroyd-B Nanoliquid over a Slippery Stretching Surface. *Ddf* 401, 164–182. doi:10.4028/www.scientific.net/ddf.401.164

Ramadhan, A. I., Azmi, W. H., Mamat, R., Hamid, K. A., and Norsakinah, S. (2019). Investigation on Stability of Tri-hybrid Nanofluids in Water-Ethylene Glycol Mixture. *Mater. Sci. Eng.* 469, 012068. doi:10.1088/1757-899X/469/1/012068

Ramadhan, A. I., Azmi, W. H., and Mamat, R. (2021). Stability and Thermal Conductivity of Tri-hybrid Nanofluids for High Concentration in Water-Ethylene Glycol (60:40). *Nanoscience & Nanotechnology-Asia* 11 (4), e270421184600. doi:10.2174/2210681210999200806153039

Ray, S. S., and Bandyopadhyay, J. (2021). Nanotechnology-enabled Biomedical Engineering: Current Trends, Future Scopes, and Perspectives. *Nanotechnology Rev.* 10, 728–743. doi:10.1515/ntrev-2021-0052

Said, Z., Sharma, P., Syam Sundar, L., Afzal, A., and Li, C. (2021). Synthesis, Stability, Thermophysical Properties and AI Approach for Predictive Modelling of Fe3O4 Coated MWCNT Hybrid Nanofluids. *J. Mol. Liquids* 340, 117291. doi:10.1016/j.molliq.2021.117291

Shahid, A., Bhatti, M. M., Ellahi, R., and Mekheimer, K. S. (2022). Numerical experiment to Examine Activation Energy and Bi-convection Carreau Nanofluid Flow on an Upper Paraboloid Porous Surface: Application in Solar Energy. *Sustainable Energ. Tech. Assessments* 52 (ID), 102029. doi:10.1016/j.seta.2022.102029

Zhao, Q., Xu, H., and Fan, T. (2015). Analysis of Three-Dimensional Boundary-Layer Nanofluid Flow and Heat Transfer over a Stretching Surface by Means of the Homotopy Analysis Method. *Boundary Value Probl.* 2015, 64. doi:10.1186/s13661-015-0327-3

Zhao, W., Karp, J. M., Ferrari, M., and Serda, R. (2011). Bioengineering Nanotechnology: towards the Clinic. *Nanotechnology* 22, 490201–490249. doi:10.1088/0957-4484/22/49/490201

Conflict of Interest: The authors declare that the research was conducted in the absence of any commercial or financial relationships that could be construed as a potential conflict of interest.